THE JOURNAL OF PHYSICAL CHEMISTRY A

Article

pubs.acs.org/JPCA

High-Pressure Studies of Bi_2S_3

Ilias Efthimiopoulos,[†] Jason Kemichick,[†] X. Zhou,[‡] Sanjay V. Khare,[§] Daijo Ikuta,[∥] and Yuejian Wang*[,†]

[†]Department of Physics, Oakland University, Rochester, Michigan, 48309, United States

[‡]Department of Chemistry and Biochemistry, University of Maryland, College Park, Maryland 20742, United States

[§]Department of Physics, University of Toledo, Toledo, Ohio 43606, United States

[∥]High Pressure Collaborative Access Team, Geophysical Laboratory, Carnegie Institution of Washington, Argonne, Illinois 60439, United States

Supporting Information

ABSTRACT: The high-pressure structural and vibrational properties of Bi_2S_3 have been probed up to 65 GPa with a combination of experimental and theoretical methods. The ambient-pressure *Pnma* structure is found to persist up to 50 GPa; further compression leads to structural disorder. Closer inspection of our structural and Raman spectroscopic results reveals notable compressibility changes in specific structural parameters of the *Pnma* phase beyond 4−6 GPa. By taking the available literature into account, we speculate that a second-order isostructural transition is realized near that pressure, originating probably from a topological modification of the Bi_2S_3 electronic structure near that pressure. Finally, the Bi^{3+} lone-electron pair (LEP) stereochemical activity decreases against pressure increase; an utter vanishing, however, is not expected until 1 Mbar. This persistence of the Bi^{3+} LEP activity in Bi_2S_3 can explain the absence of any structural transitions toward higher crystalline symmetries in the investigated pressure range.

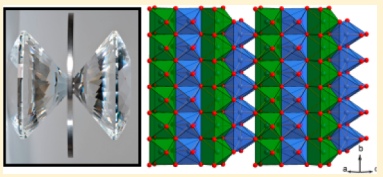

1. INTRODUCTION

The mineral bismuthinite (Bi_2S_3) is a well-known binary semiconductor with an optical band gap $E_g \sim 1.3$ eV.[1,2] This material constitutes a promising candidate for optoelectronic[3] and photovoltaic[4] applications. At ambient conditions, Bi_2S_3 adopts an orthorhombic structure (*Pnma*, $Z = 4$, U_2S_3-type) with mixed 7-fold [Bi(1)] and 8-fold [Bi(2)] cationic coordinations (Figure 1). This *Pnma* phase can be described as a layered structure, with alternating blocks of Bi−S polyhedral units stacked perpendicular to the short *b*-axis (Figure 1).

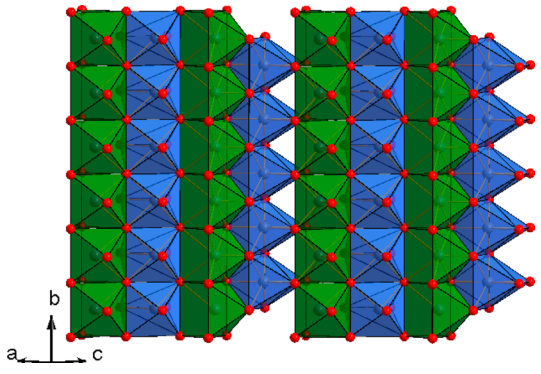

Figure 1. A polyhedral view along [101] of the layered structure of Bi_2S_3 at ambient conditions (*Pnma*, $Z = 4$). The blue, green, and red spheres correspond to the Bi(1), Bi(2), and S ions, respectively. The blue and green polyhedra stand for the Bi(1)S_7 and the Bi(2)S_{7+1} units.

By substituting sulfur in Bi_2S_3 with selenium (Bi_2Se_3) or tellurium (Bi_2Te_3), one falls into a completely different structural class. In particular, both Bi_2Te_3 and Bi_2Se_3 compounds adopt a rhombohedral structure ($R\bar{3}m$, $Z = 3$) at ambient conditions,[5,6] which is made up of Bi(Se,Te)$_6$ octahedral layers piled up along the *c*-axis. Interestingly, both of these materials were shown to exhibit topological properties at ambient pressure.[7,8]

The quasi two-dimensional structure of these Bi-based chalcogenides makes the physical properties of these systems susceptible to strain. Indeed, it is well-established that application of external pressure enhances the thermoelectric performance of these materials due to a pressure-induced electronic topological transition.[9] More recent high-pressure investigations unraveled a rich phase diagram for these materials under pressure, with a plethora of novel structures of higher cationic coordinations[5,6,10−12] and concominant electronic transitions[10,13,14] arising upon compression. Even though the effect of pressure on the structural properties of Bi_2Te_3 and Bi_2Se_3 compounds has been studied extensively, the denser Bi_2S_3 has not received similar attention owing probably to the lack of topological properties.

The only known high-pressure work to date on Bi_2S_3 is a structural study up to 10 GPa.[15] The main outcome of this investigation was the persistence of the *Pnma* phase up to that pressure. In addition, the Bi−S polyhedral units became more symmetric, associated closely to a decrease of the Bi^{3+} lone-

Received: December 19, 2013
Revised: February 10, 2014
Published: February 10, 2014

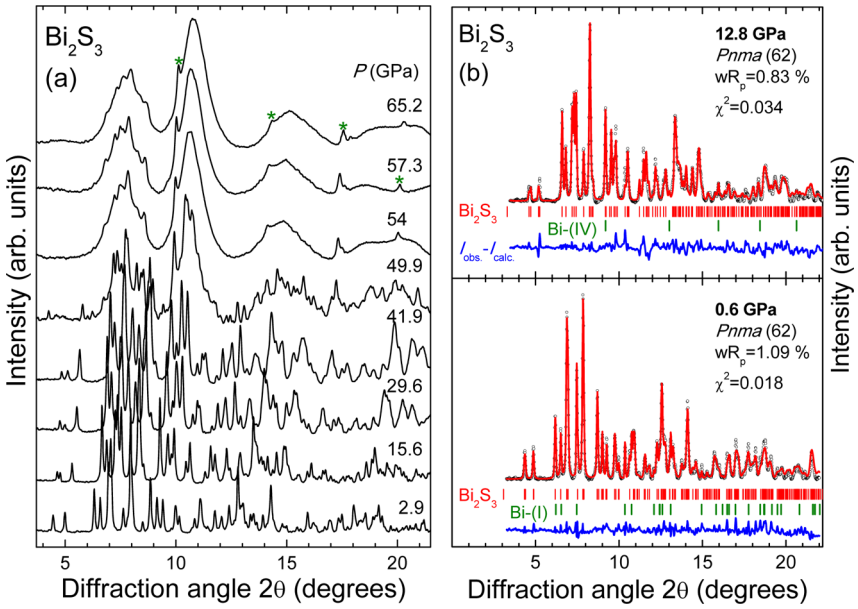

Figure 2. (a) XRD patterns of Bi_2S_3 at selected pressures (T = 300 K, λ = 0.4246 Å). Asterisks mark the Bragg peaks of the Bi impurity. Background has been subtracted for clarity. (b) Examples of Rietveld refinements performed with Le Bail fit due to the strong texture at two different pressures. Dots correspond to the measured spectra and the red solid lines represent the best refinements. The difference spectra between the measured and the refined patterns are depicted too (blue lines). Vertical ticks mark Bragg peak positions.

electron pair (LEP) stereochemical activity under pressure.[15,16] The complete suppression of LEP activity was estimated above 20 GPa; such vanishing may induce a structural transition toward a phase of higher symmetry, accompanied by changes in the electronic properties of Bi_2S_3.[17,18] Partly motivated by this possibility, and given the *Pnma*-bcc transition observed recently for isostructural Sb_2Se_3 above 50 GPa,[19] we have expanded the pressure-range of the structural on Bi_2S_3 up to 65 GPa, complemented by high-pressure Raman spectroscopic studies up to ∼28 GPa. Overall, the *Pnma* phase is stable up to 50 GPa, with structural disorder initiating beyond that pressure. The Bi^{3+} LEP activity is decreasing in a nonmonotonous way, with a complete suppression expected above 1 Mbar (Appendix in the Supporting Information (SI)). On the other hand, a closer inspection of the structural and vibrational properties at lower pressures reveals notable compressibility changes of specific structural parameters above 4 GPa. These pressure-induced changes are reminiscent of the second-order isostructural transitions reported for Bi_2Te_3, Bi_2Se_3, and Sb_2Te_3 compounds at low pressures.[20]

2. EXPERIMENTAL AND COMPUTATIONAL DETAILS

Bi_2S_3 was available in polycrystalline form (Alfa-Aesar, 99.9% purity). Pressure was generated with a gasketed symmetric diamond anvil cell (DAC), equipped with a set of diamonds with 300 μm culet diameter. The ruby luminescence method was employed for pressure calibration.[21]

The monochromatic angle-dispersive powder X-ray diffraction (XRD) measurements under pressure were performed at the 16BM-D beamline of the High Pressure Collaborative Access Team's facility, at the Advanced Photon Source of Argonne National Laboratory (APS-ANL). The X-ray beam wavelength was λ = 0.4246 Å. The XRD patterns were collected with a MAR 345 Image Plate detector. The sample−detector distance and the geometrical parameters were calibrated with a CeO_2 standard from NIST. The intensity versus 2θ spectra were processed with the FIT2D software.[22] Refinements were performed with the GSAS+EXPGUI software packages.[23,24] The P−V data were fitted with the Birch−Murnaghan equation of state (B-M EOS).[25] Helium was employed as a pressure transmitting medium (PTM); the compressed gas loading took place at the gas-loading system of GeoSoilEnviroCARS[26] (Sector 13, APS-ANL).

The high-pressure Raman measurements were conducted with a solid-state laser (λ = 532 nm) coupled to a single-stage spectrometer and a charge-coupled device. The spectral resolution was 2 cm^{-1} and the lowest resolvable frequency ∼80 cm^{-1}. The incident laser power was 2 mW outside the DAC, and the size of the laser spot was approximately 30 μm. Both helium and a mixture of methanol−ethanol−water (16:3:1) served as PTM in separate experimental runs.

All of the ab initio calculations are performed by using the Vienna *Ab-initio* Simulation Package (VASP)[27−29] codes within the projector augmented wave general gradient approximation (PAW-GGA) to density functional theory (DFT).[30,31] The electron-ion interactions are treated by ultrasoft-Vanderbilt type pseudo potentials[32] as supplied by Kresse et al.[33] A cutoff energy, 350 eV, is applied to the valence electronic wave functions expanded in a plane-wave basis set for the orthorhombic Bi_2S_3. A Monkhorst-Pack[34] generated k-point grid, 4 × 11 × 5, which matches the reciprocal lattice vector lengths, was used for the Brillouin-zone integrations in all calculations. Tests using the cutoff energy and k-points mentioned above reached a convergence better than 1 meV. The lattice constants and atomic positions for each configuration with different pressures are obtained by fully relaxing all atoms and lattice constants until a force convergence to less than 0.01 eV/Å was achieved, similar to an earlier work.[35] Additional crystal-chemical calculations were performed with IVTON software.[36] It should be emphasized that there exist several settings for *Pnma*; here we use the same *Pnma* setting as in refs 15, 19, and 37 (setting #1).

dx.doi.org/10.1021/jp4124666 | J. Phys. Chem. A 2014, 118, 1713−1720

3. RESULTS AND DISCUSSION

3.1. Structure under Pressure. *3.1.1. X-ray Diffraction Study.* In Figure 2a we present selected XRD patterns of Bi_2S_3 at various pressures, whereas examples of refinements are depicted in Figure 2b. Due to strong texture effects, only the lattice parameters could be extracted. In addition, analysis of the XRD patterns revealed the presence of elemental bismuth as an impurity phase at all pressures from the beginning of the experiment. The structural evolution of Bi is well-established:[38,39] the starting rhombohedral structure (Bi−I) transforms into a distorted cubic phase (Bi−II) at 2.55 GPa, whereas above 2.7 GPa it adopts a bct tetragonal structure (Bi−III). Finally, Bi adopts a bcc phase at 8 GPa (Bi−IV), which persists up to 2 Mbar[40] (asterisks in Figure 2a). Therefore, both Bi_2S_3 and Bi phases were taken into account for all of the XRD refinements (Figure 2b).

Upon compression, Bi_2S_3 retains the *Pnma* phase up to ∼50 GPa. Above that pressure, the XRD patterns are dominated by broad Bragg features up to 65 GPa (Figure 2a). This pressure-induced Bragg peak broadening in the XRD patterns of Bi_2S_3 can originate from various effects, such as structural disorder/amorphization, nonhydrostatic conditions, grain size effects, and/or other structural defects induced upon compression.[41,42] Given, however, the trends of Bi_2Te_3,[5,10] Bi_2Se_3,[6] Sb_2Te_3,[43,44] and Sb_2Se_3[19] compounds toward disordered structures under presure, we interpret this Bragg peak broadening as a sign of pressure-induced structural disorder in Bi_2S_3. Interestingly, a similar disorder precedes the *Pnma*-bcc structural transition in Sb_2Se_3 under high pressure.[19] Due to time constraints, the decompression cycle of the experiment could not be performed; this will be the subject of a future study.

From the pressure dependence of the lattice parameters, we can observe that the compressibility of the *Pnma* structure is anisotropic (Figure 3a). In particular, the long *a*- and *c*-axes exhibit similar behavior upon increasing pressure, with the *c*-axis being generally more compressible than the *a*-direction. As for the short *b*-axis, it is the stiffer lattice constant with an almost linear (within error) pressure-change up to 50 GPa. When comparing the zero-pressure compressibility of the lattice constants $\beta_0 = l_0^{-1}(\partial l/\partial P)_{P=0}$, ($l_0$ is the zero-pressure value of the respective unit-cell axis) between isostructural Bi_2S_3 and Sb_2Se_3,[19] we find that Bi_2S_3 is "softer" than Sb_2Se_3 along the *a*-axis. On the other hand, both compounds exhibit similar compressibilities along the *b*- and *c*- directions, with the *b*-axis being the most incompressible lattice parameter in both cases.

By taking a closer look at the lattice constant ratios (Figure 3b), we can observe some interesting changes in the pressure dependence of both *a*/*b* and *a*/*c* near 4 GPa. More precisely, the initially "softer" *a*-axis reaches the *b*-axis in terms of compressibility above 4 GPa, whereas it becomes stiffer than the *c*-axis beyond that pressure. This axial compressibility change is directly linked to changes of respective interatomic parameters, as we discuss in more detail below. In Figure 3c we display the *P*-*V* data for the *Pnma* phase of Bi_2S_3. By employing the experimental zero-pressure volume per formula unit V_0/Z = 125.4 Å^3, we acquire a bulk modulus B_0 = 38.9(8) GPa and its pressure derivative B'_0 = 5.5(1) via the B-M EOS fitting. The obtained B_0 and B'_0 values are consistent with those of isostructural Sb_2Se_3[19] and Sb_2S_3[37] compounds.

3.1.1. Theoretical Results. Turning now to our computational results, we have plotted the theoretically derived structural parameters of Bi_2S_3, using PAW-GGA, as a function of pressure alongside the experimental data (solid lines in Figure 3). It can be observed that an overall excellent agreement between theory and experiment is achieved, with the calculated lattice parameters being slightly overestimated compared to the experimental data (∼1%) as expected for GGA.[45] The compressibility changes for both *a*/*b* and *a*/*c* lattice constant ratios are reproduced by our computations (Figure 3b). Finally, the elastic parameters obtained from the calculated *P*−*V* data (Figure 3c) are V_0/Z = 127.9 Å^3, B_0 = 36.5 GPa, and B'_0 = 5.9, in very good agreement with the experimental results.

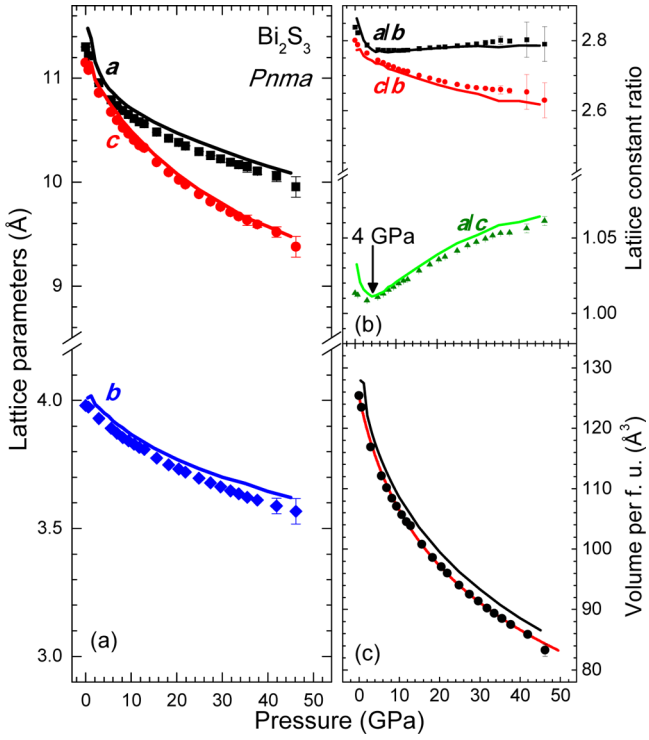

Figure 3. Plot of the (a) lattice parameters, (b) lattice constant ratios, and (c) unit cell volume per formula unit as a function of pressure for the *Pnma* phase of Bi_2S_3. The closed symbols and the solid lines represent experimental and computed data, respectively. The red solid line in panel c represents the fitted B-M EOS function.

In order to get a more comprehensive understanding of the effect of pressure on the structural properties of Bi_2S_3, we have additionally calculated the positional coordinates of all ions within the *Pnma* unit cell at various pressures, from DFT computational data (Table S1 in the SI). By employing these atomic parameters, we have derived the pressure dependence of the various Bi−S bond lengths. In Figure 4a,b we plot the pressure dependence of the theoretically derived lattice constants and selected interatomic Bi−S bond lengths of Bi_2S_3 up to 10 GPa. From Figure 4a, we can clearly observe the compressibility change of the orthorhombic *a*-axis above 4 GPa mentioned above; both *b*- and *c*-axes, on the other hand, do not show any anomalous behavior within this pressure range. This compressibility change of the *a*-axis is linked to modifications of the pressure dependence of distinctive bond lengths. In particular, the long Bi(1)−S(2) and the short Bi(2)−S(1) bond lengths experience subtle compressibility changes above 4 GPa. The most pronounced pressure-related effect, however, is exhibited by the Bi(1)−S(3) bond distance, which undergoes a reversal in its pressure dependence above 4 GPa (Figure 4b).

dx.doi.org/10.1021/jp4124666 | J. Phys. Chem. A 2014, 118, 1713−1720

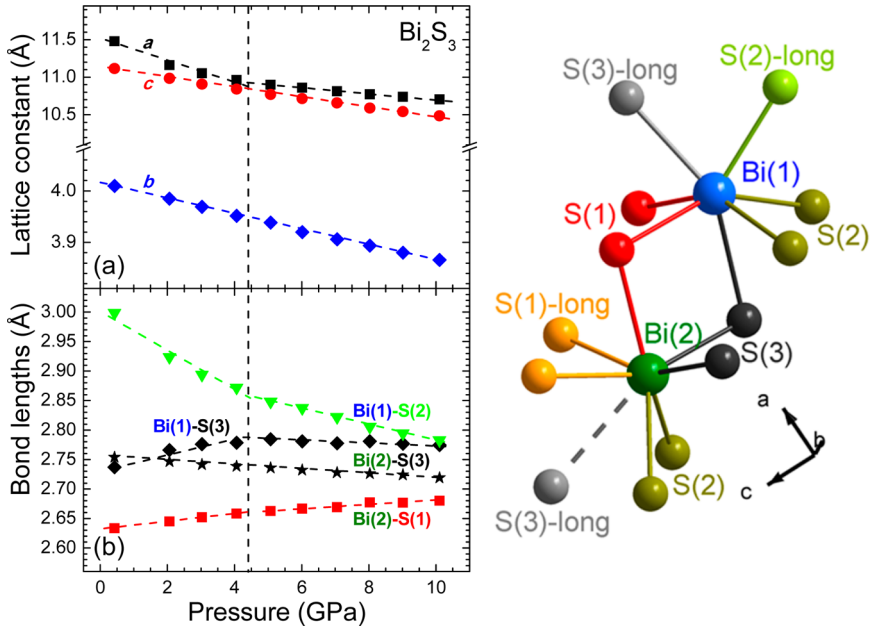

Figure 4. Plot of the (a) lattice constants and (b) selected Bi−S bond lengths of Bi_2S_3 up to 10 GPa. In order to be consistent with the pressure values, we have employed the computed structural parameters. The vertical dashed line marks the onset of the compressibility changes. The nomenclature of the various Bi and S ions is also provided.

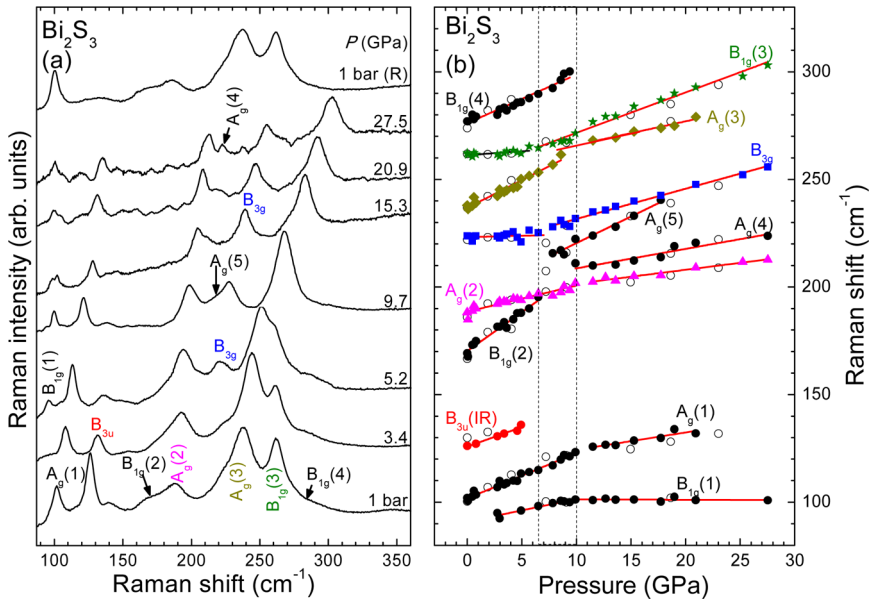

Figure 5. (a) Raman spectra of Bi_2S_3 at selected pressures (λ = 532 nm, T = 300 K). (b) Raman mode frequency evolution against pressure. Solid and open circles correspond to data collected upon compression and decompression, respectively. Solid lines represent least-squares fits. The dashed area marks the pressure range of subtle Raman-related changes.

These distinctive compressibility changes of specific structural parameters are reminiscent of second-order isostructural transitions observed in related layered materials,[20] i.e., structural transitions without any symmetry change and volume discontinuities. Thus, in a similar fashion, we attribute the observed compressibility changes in Bi_2S_3 above 4 GPa to a *second-order isostructural transition*.

As for the effect of pressure on the Bi^{3+} lone-electron pair stereochemical activity, a nonmonotonous suppression is observed up to 45 GPa; a complete vanishing of the LEP activity, however, is expected above 1 Mbar (Appendix). Therefore, this persistence of the LEP activity of Bi_2S_3 can account well for the absence of any structural transitions toward higher crystalline symmetries within the investigated pressure range.

3.2. High-Pressure Raman Investigation. Raman spectroscopy constitutes a more sensitive probe for detecting isostructural transitions. For example, it has been shown that in Bi_2Te_3,[46] Bi_2Se_3,[47] and Sb_2Te_3[48] the changes of Raman-active modes' pressure coefficients and linewidths can be taken as evidence of the respective isostructural transitions. In order to look for similar pressure-induced effects in Bi_2S_3, we have conducted high-pressure Raman investigations up to 28 GPa. A

dx.doi.org/10.1021/jp4124666 | J. Phys. Chem. A 2014, 118, 1713−1720

sum of thirty Raman-active modes are expected for the orthorhombic *Pnma* phase[49]

$$\Gamma = 10A_g + 5B_{1g} + 10B_{2g} + 5B_{3g}$$

At ambient pressure, we can resolve nine broad bands in our Raman spectra (Figure 5 and Table 1). Eight of the observed features are Raman-active modes, in agreement with previous reports.[49−51] On the other hand, the feature at ∼125 cm^{-1} (B_{3u}, Figure 5 and Table 1) has been assigned to an infrared (IR)-active mode.[49] Since the noncentrosymmetric *Pnma* permits the existence of both Raman- and IR-active modes in the Raman spectra, and given the significant variation of this feature intensity-wise upon sample choice, the assignment of the band at ∼125 cm^{-1} as an IR-active mode seems plausible and is adopted in this work.

Table 1. Mode Assignment,[49] Raman Mode Frequencies, Pressure Coefficients, and the Mode Gruneisen Parameters γ of the Raman Features of Bi_2S_3[a]

P_{Tr} (GPa)	mode symmetry	ω_{Tr} (cm^{-1})	$\partial\omega/\partial P$ (cm^{-1}/GPa)	γ
1 bar	B_{1g} (1)	90.9	1.1	0.47
	A_g (1)	101.8	2.1	0.8
	B_{3u} (IR)	125.8	1.8	0.56
	B_{1g} (2)	170.2	3.6	0.82
	A_g (2)	188.6	1.2	0.25
	B_{3g}	223.2	0.1	0.02
	A_g (3)	236.8	2.6	0.43
	B_{1g} (3)	261.3	0.4	0.06
	B_{1g} (4)	276.1	2.3	0.32
10 GPa	B_{1g} (1)	101.3	−0.02	−0.02
	A_g (1)	124.3	0.8	0.58
	A_g (2)	201.1	0.6	0.27
	B_{3g}	231.6	1.4	0.55
	A_g (3)	266	1.1	0.38
	B_{1g} (3)	271.8	1.9	0.63
	A_g (4)	208.6	0.9	0.39
	A_g (5)	220.7	2.5	1.03

[a]The pressure depencence of the Raman-active modes is described by the relation $\omega(P) = \omega_{Tr} + \alpha P_{Tr}$. Mode Gruneisen parameters γ are determined from the relation $\gamma = (B_{Tr}/\omega_{Tr}) \times (\partial\omega/\partial P)$, where ω_{Tr} and the bulk modulus B_{Tr} are evaluated at the respective transition pressure point P_{Tr}. The bulk moduli values 38.9 GPa (P_{Tr} = 1 bar) and 90.6 GPa (P_{Tr} = 10 GPa, extrapolated) were employed.

Upon increasing pressure, several effects can be observed in the Raman spectra within the 6−10 GPa pressure range (Figure 5b). In particular, the $B_{1g}(2)$ mode merges with its neighboring $A_g(2)$ Raman band and cannot be resolved above 7 GPa. In addition, two new low-intensity features, i.e., $A_g(4)$ and $A_g(5)$ are observed beyond 10 GPa (Figure 5b). Since no long-range structural transition takes place near that pressure according to our XRD study, these modes are most likely overlapping ambient-pressure Raman bands which become "visible" under compression, instead of novel Raman features due to a subtle structural modification. This scenario appears plausibe if we take into account that the estimated zero-pressure frequencies for both of these modes (Table 1) are well reproduced from the theoretical modeling of the Bi_2S_3 vibrational properties.[49] Furthermore, changes in the pressure dependence of almost every observable Raman-active mode can be detected above 10 GPa (Figure 5b and Table 1). Since we have also used helium as the PTM, we can most likely exclude any nonhydrostatic effects as the origin behind these pressure-induced compressibility changes. Therefore, we attribute these changes to variations of the respective force constants within the 6−10 GPa pressure range.

With the exception of the low-frequency $A_g(1)$ mode, most of the compressibility changes in the Raman-active modes take place just above 6 GPa (Figure 5b), very close to the compressibility changes of the structural parameters (>4 GPa, Figure 4). Since these compressibility changes roughly coincide in terms of pressure values, it is only reasonable to assume that a direct link exists. Even though a line width analysis of these modes[52] would provide more valuable information, we can still interpret the observed compressibility changes of the Raman-active modes of Bi_2S_3 as additional evidence of a pressure-induced isostructural transition occurring within the 4−6 GPa pressure range.

Finally, we discuss the possible contamination of our Raman spectra from Bi impurities as observed in the XRD measurements. Elemental Bi exhibits low-frequency modes below 100 cm^{-1}.[39] Even though the low-frequency $A_g(1)$ mode of Bi_2S_3 lies suspiciously close with the A_{1g} band of Bi−I, the two features exhibit opposite pressure dependence.[39] In addition, Bi can also oxidize and form the a-Bi_2O_3 phase under laser irradiation.[51] Given, however, that the strongest Raman features of a-Bi_2O_3 reside in the 300−500 cm^{-1} frequency range,[53] we can also exclude its presence in our Raman spectra (Figure 5a).

3.3. Structural Systematics of the A_2B_3 Series under Pressure. Even though the high-pressure structural behavior of the A_2B_3 (A^{3+} = Sb, Bi; B^{2-} = S, Se, Te) family has been investigated for many years (for a review, see ref 20), the high-pressure phases have been solved only recently through combined experimental and theoretical efforts.[5,12,44] In particular, the heaviest member of this series, i.e., Bi_2Te_3 undergoes three structural transitions up to 52 GPa.[5,10,11] In particular, the starting $R\bar{3}m$ phase transforms into a monoclinic structure ($C2/m$, Z = 4) with 7-fold cationic coordination above 8 GPa. Upon further pressure increase, a second monoclinic structure ($C2/c$, Z = 4) with 8-fold coordination appears for a narrow pressure range (13.4−14.4 GPa). Finally, a disordered bcc alloy ($Im\bar{3}m$, Z = 2) is stabilized above 14.4 GPa; this disordered phase persists up to 52 GPa. A similar sequence of pressure-induced structural transitions is reported for Sb_2Te_3.[43,44,54]

As for the structural behavior of Bi_2Se_3 under pressure, the starting $R\bar{3}m$ phase also adopts the $C2/m$ phase at ∼10 GPa.[6,12] Upon further pressure increase, however, observations are somewhat diverse. In particular, Bi_2Se_3 was shown to transform from the first high-pressure $C2/m$ phase directly into a body-centered tetragonal structure ($I4/mmm$, Z = 2) above 25 GPa;[6] upon decompression, an amorphous phase is recovered. Given sufficient relaxation time, the orthorhombic Bi_2Se_3−II phase (isostructural to Bi_2S_3) forms from the amorphous material.[6] In ref 12, on the other hand, Bi_2Se_3 is found to exhibit the same structural sequence as the Bi_2Te_3 and Sb_2Te_3 compounds, i.e., $R\bar{3}m \rightarrow C2/m \rightarrow C2/c$. Upon further compression, a novel monoclinic phase ($C2/m$, Z = 4) was observed. This third high-pressure phase is the densest structure reported so far for these materials, since the Bi cations adopt a mixed 9-fold and 10-fold coordination with respect to the Se anions. The absence of the disordered bcc phase was attributed to the large differences in the atomic radii and electronegativity between Bi and Se.[12]

Turning now to the orthorhombic Sb_2Se_3, Sb_2S_3, and Bi_2S_3 compounds, similar high-pressure studies are scarce. Earlier

dx.doi.org/10.1021/jp4124666 | J. Phys. Chem. A 2014, 118, 1713−1720

structural investigations on Sb_2S_3[37] and Bi_2S_3[15] up to 10 GPa, as well as a recent study on Bi_2Se_3–II up to 26 GPa[6] did not report any structural transitions for the *Pnma* phase up to those pressures. On the other hand, our recent high-pressure structural study on Sb_2Se_3 revealed the transformation of the *Pnma* phase into a disordered bcc structure above 55 GPa,[19] reminiscent of the end-phases of Bi_2Te_3[5,10,11] and Sb_2Te_3[43,44,54] under pressure. In the case of Bi_2S_3, we have found that the ambient-pressure *Pnma* phase persists all the way up to 50 GPa (Figure 2b). Further compression results in a significant broadening of the Bragg peaks in the XRD patterns, thus signaling the onset of structural disorder. Such disorder can generally be accounted for by two mechanisms:[42] (a) the disordered phase may be a transient of a structural transition into another crystalline phase, which cannot be formed with a high crystalline quality due to kinetic barriers, or (b) the tendency of the material to decompose into its constituents.

Regarding the latter, elemental dissociation is favored in terms of volume at these pressures:

$$V/Z(Bi_2S_3) > 2V_{at}(Bi) + 3V_{at}(S)$$

with $V/Z(Bi_2S_3)$ = 85.8 Å^3, $V_{at}(Bi) \approx 22$ Å^3 (Bi–IV),[40] and $V_{at}(S)$ = 13.2 Å^3 (S–III)[55] at 42 GPa. Given, however, the trends of Bi_2Te_3,[5,10,11] Sb_2Te_3,[43,44,54] and Sb_2Se_3[19] compounds toward high-pressure disordered phases instead of elemental decomposition, the scenario of a kinetically hindered structural transition in Bi_2S_3 appears more plausible; a combined high-pressure and high-temperature structural study will be needed in order to resolve this matter. Considering, nevertheless, the structural trends of the A_2B_3 series under pressure, we can expect that this new structure will most likely exhibit higher cationic coordinations. We can also propose some possible structural candidates for Bi_2S_3: (1) the monoclinic high-pressure phase of Bi_2Te_3,[5,10] Sb_2Te_3,[44,54] and Bi_2Se_3[6,12] ($C2/c$, Z = 4) with 8-fold cationic coordination, (b) the cubic Th_3P_4-type structure ($I\bar{4}3d$, Z = 4) with 8-fold cationic coordination, a common polymorph for rare-earth sulfides,[56] and (c) the mixed 9/10-fold high-pressure structure found recently for Bi_2Se_3.[12]

Finally, we would like to add some thoughts on the possible microscopic origin behind the isostructural transition of Bi_2S_3 observed within 4–6 GPa (Figures 4 and 5). It has been established that an electronic topological transition (ETT) takes place for all Bi_2Te_3, Bi_2Se_3, and Sb_2Te_3 compounds near 4 GPa.[20] These ETTs are evidenced from the compressibility changes of the c/a lattice constant ratios, i.e., they are treated as second-order isostructural transitions. In addition, detailed high-pressure Raman studies of Bi_2Te_3,[46] Bi_2Se_3,[47] and Sb_2Te_3[48] compounds revealed marked changes of their Raman-active modes near the ETT in terms of pressure coefficients and linewidths. Interestingly, a recent high-pressure Raman investigation on Sb_2Se_3 reported also an ETT below 3 GPa;[57] the Raman spectra, however, suffered from PTM contamination, thus making this result questionable (for a detailed discussion, see ref 19).

By taking into account the aforementioned discussion, we tend to ascribe the compressibility changes observed in Bi_2S_3, i.e., the isostructural transition at 4–6 GPa, to a topological change of its electronic structure near that pressure. Even though the aforementioned materials (Bi_2Te_3, Sb_2Te_3, Bi_2Se_3) crystallize in the $R\bar{3}m$ phase, their band structures are very similar with that of Bi_2S_3.[2,14,58,59] Therefore, the possibility of a pressure-induced ETT above 4 GPa appears reasonable. Finally, we should mention that a similar axial compressibility change was detected in isostructural Sb_2Se_3 close to 4 GPa;[19] current efforts are focusing on the careful analysis of the Sb_2Se_3 Raman spectra near that pressure value.

4. CONCLUSIONS

In summary, the ambient-pressure *Pnma* structure of Bi_2S_3 persists up to 50 GPa; beyond that pressure, we observed significantly broadened features in the XRD patterns. Considering the structural trends of Sb_2Se_3,[19] Bi_2Te_3,[5,11] Bi_2Se_3,[6] and Sb_2Te_3[43,44] compounds upon compression, we interpret this behavior as a sign of pressure-induced structural disorder. In addition, clear compressibility changes in several interatomic bond lengths and Raman-active modes were detected within the 4–6 GPa pressure range. By taking into account earlier reports,[20] we assign these compressibility changes to a *second-order isostructural transition*, arising probably from changes in the electronic structure of Bi_2S_3. Finally, pressure is found to decrease the Bi^{3+} LEP activity (Appendix); a complete suppression, however, is not expected until 1 Mbar.

■ ASSOCIATED CONTENT

Ⓢ Supporting Information

The calculated atomic positions, the derived Bi–S bond lengths, and the discussion of the pressure effect on the lone-pair stereochemical activity are included in the Supporting Information. This information is available free of charge via the Internet at http://pubs.acs.org.

■ AUTHOR INFORMATION

Corresponding Author

*E-mail: ywang235@oakland.edu; Phone: 248-370-3423; Fax: 248-370-3408.

Notes

The authors declare no competing financial interest.

■ ACKNOWLEDGMENTS

Portions of this work were performed at HPCAT (Sector 16), Advanced Photon Source (APS), Argonne National Laboratory (ANL). HPCAT operations are supported by DOE-NNSA under Award No. DE-NA0001974 and DOE-BES under Award No. DE-FG02-99ER45775, with partial instrumentation funding by NSF. APS is supported by DOE-BES, under Contract No. DE-AC02-06CH11357. We thank the Ohio Supercomputer Center (OSC) and NSF grant CNS 0855134 for computing resources. We thank the National Science Foundation grant CMMI 1234777 for funding as well.

The compressed helium gas loading was performed at GeoSoilEnviroCARS (Sector 13), at APS-ANL. GSECARS is supported by the National Science Foundation-Earth Sciences (EAR-0217473), Department of Energy-Geosciences (DE-FG02-94ER14466) and the State of Illinois. We would like to acknowledge Dr. S. Tkachev for his help with the DAC loading.

■ REFERENCES

(1) Sharma, Y.; Srivastava, P.; Dashora, A.; Vadkhiya, L.; Bhayani, M. K.; Jain, R.; Jani, A. R.; Ahuja, B. L. Electronic Structure, Optical Properties and Compton Profiles of Bi_2S_3 and Bi_2Se_3. *Solid State Sci.* **2012**, *14*, 241–249.

(2) Filip, M. R.; Patrick, C. E.; Giustino, F. GW Quasiparticle Band Structures of Stibnite, Antimonselite, Bismuthinite, and Guanajuatite. *Phys. Rev. B* **2013**, *87*, 205125.

(3) Konstantatos, G.; Levina, L.; Tang, J.; Sargent, E. H. Sensitive Solution-Processed Bi_2S_3 Nanocrystalline Photodetectors. *Nano Lett.* **2008**, *8*, 4002−4006.
(4) Pawar, S. H.; Bhosale, P. N.; Uplane, M. D.; Tamhankar, S. Growth of Bi_2S_3 Film Using a Solution-Gas Interface Technique. *Thin Solid Films* **1983**, *110*, 165−170.
(5) Zhu, L.; Wang, H.; Wang, Y.; Lv, J.; Ma, Y.; Cui, Q.; Zou, G. Substitutional Alloy of Bi and Te at High Pressure. *Phys. Rev. Lett.* **2011**, *106*, 145501.
(6) Zhao, J.; Liu, H.; Ehm, L.; Dong, D.; Chen, Z.; Gu, G. High-Pressure Phase Transitions, Amorphization, and Crystallization Behaviors in Bi_2Se_3. *J. Phys.: Condens. Matter* **2013**, *25*, 125602.
(7) Chen, Y. L.; Analytis, J. G.; Chu, J. H.; Liu, Z. K.; Mo, S. K.; Qi, X. L.; Zhang, H. J.; Lu, D. H.; Dai, X.; Fang, Z.; et al. Experimental Realization of a Three-Dimensional Topological Insulator, Bi_2Te_3. *Science* **2009**, *325*, 178−181.
(8) Zhang, H. J.; Liu, C. X.; Qi, X. L.; Dai, X.; Fang, Z.; Zhang, S. C. Topological Insulators in Bi_2Se_3, Bi_2Te_3 and Sb_2Te_3 with a Single Dirac Cone on the Surface. *Nat. Phys.* **2009**, *5*, 438−442.
(9) Ovsyannikov, S. V; Shchennikov, V. V. High-Pressure Routes in the Thermoelectricity or How One Can Improve a Performance of Thermoelectrics. *Chem. Mater.* **2010**, *22*, 635−647.
(10) Zhang, S. J.; Zhang, J. L.; Yu, X. H.; Zhu, J.; Kong, P. P.; Feng, S. M.; Liu, Q. Q.; Yang, L. X.; Wang, X. C.; Cao, L. Z.; et al. The Comprehensive Phase Evolution for Bi_2Te_3 Topological Compound as Function of Pressure. *J. Appl. Phys.* **2012**, *111*, 112630.
(11) Einaga, M.; Ohmura, A.; Nakayama, A.; Ishikawa, F.; Yamada, Y.; Nakano, S. Pressure-Induced Phase Transition of Bi_2Te_3 to a Bcc Structure. *Phys. Rev. B* **2011**, *83*, 92102.
(12) Liu, G. T.; Zhu, L.; Ma, Y. M.; Lin, C. L.; Liu, J. Stabilization of 9/10-Fold Structure in Bismuth Selenide at High Pressures. *J. Phys. Chem. C* **2013**, *117*, 10045−10050.
(13) Hamlin, J. J.; Jeffries, J. R.; Butch, N. P.; Syers, P.; Zocco, D. A.; Weir, S. T.; Vohra, Y. K.; Paglione, J.; Maple, M. B. High Pressure Transport Properties of the Topological Insulator Bi_2Se_3. *J. Phys.: Condens. Matter* **2012**, *24*, 35602.
(14) Zhang, J. L.; Zhang, S. J.; Weng, H. M.; Zhang, W.; Yang, L. X.; Liu, Q. Q.; Feng, S. M.; Wang, X. C.; Yu, R. C.; Cao, L. Z.; et al. Pressure-Induced Superconductivity in Topological Parent Compound Bi_2Te_3. *Proc. Natl. Acad. Sci. U. S. A.* **2011**, *108*, 24−28.
(15) Lundegaard, L. F.; Makovicky, E.; Boffa-Ballaran, T.; Balic-Zunic, T. Crystal Structure and Cation Lone Electron Pair Activity of Bi_2S_3 between 0 and 10 GPa. *Phys. Chem. Miner.* **2005**, *32*, 578−584.
(16) Olsen, L. A.; Lopez-Solano, J.; Garcia, A.; Balic-Zunic, T.; Makovicky, E. Dependence of the Lone Pair of Bismuth on Coordination Environment and Pressure: An Ab Initio Study on$Cu_4Bi_5S_{10}$ and Bi_2S_3. *J. Solid State Chem.* **2010**, *183*, 2133−2143.
(17) Winkler, B.; Milman, V.; Lee, M.-H. Pressure-Induced Change of the Stereochemical Activity of a Lone Electron Pair. *J. Chem. Phys.* **1998**, *108*, 5506−5509.
(18) Walsh, A.; Watson, G. W. Influence of the Anion on Lone Pair Formation in Sn(II) Monochalcogenides: A DFT Study. *J. Phys. Chem. B* **2005**, *109*, 18868−18875.
(19) Efthimiopoulos, I.; Zhang, J. M.; Kucway, M.; Park, C.; Ewing, R. C.; Wang, Y. Sb_2Se_3 under Pressure. *Sci. Rep.* **2013**, *3*, 2665.
(20) Manjon, F. J.; Vilaplana, R.; Gomis, O.; Perez-Gonzalez, E.; Santamaria-Perez, D.; Marin-Borras, V.; Segura, A.; Gonzalez, J.; Rodriguez-Hernandez, P.; Munoz, A.; et al. High-Pressure Studies of Topological Insulators Bi_2Se_3, Bi_2Te_3, and Sb_2Te_3. *Phys. Status Solidi B* **2013**, *250*, 669−676.
(21) Mao, H. K.; Xu, J.; Bell, P. M. Calibration of the Ruby Pressure Gauge to 800 kbar under Quasi-hydrostatic Conditions. *J. Geophys. Res.* **1986**, *91*, 4673−4676.
(22) Hammersley, A.; Svensson, S.; Hanfland, M.; Fitch, A.; Hausermann, D. Two-dimensional Detector Software: From Real Detector to Idealised Image or Two-theta Scan. *High Pressure Res.* **1996**, *14*, 235−248.
(23) Toby, B. H. EXPGUI, a Graphical User Interface for GSAS. *J. Appl. Crystallogr.* **2001**, *34*, 210−213.
(24) Von Dreele, R. B.; Larson, A. C. Los Alamos National Laboratory *Report No. LAUR 86-748*, 1994.
(25) Birch, F. Finite Elastic Strain of Cubic Crystals. *Phys. Rev.* **1947**, *71*, 809.
(26) Rivers, M.; Prakapenka, V. B.; Kubo, A.; Pullins, C.; Jacobsen, C. M. H. S. D. The COMPRES/GSECARS Gas-Loading System for Diamond Anvil Cells at the Advanced Photon Source. *High Press. Res.* **2008**, *28*, 273−292.
(27) Kresse, G. *Ab Initio Molekular Dynamik Fur Flussige Metalle*. Thesis, Vienna University of Technology, 1993.
(28) Kresse, G.; Furthmüller, J. Efficient Iterative Schemes for Ab Initio Total-Energy Calculations Using a Plane-Wave Basis Set. *Phys. Rev. B* **1996**, *54*, 11169−11186.
(29) Kresse, G.; Hafner, J. Ab Initio Molecular-Dynamics for Liquid Metals. *Phys. Rev. B* **1993**, *47*, 558.
(30) Kohn, W.; Sham, L. J. Quantum Density Oscillations in an Inhomogeneous Electron Gas. *Phys. Rev.* **1965**, *137*, A1697.
(31) Hohenberg, P.; Kohn, W. Inhomogeneous Electron Gas. *Phys. Rev.* **1964**, *136*, B864.
(32) Vanderbilt, D. Soft Self-Consistent Pseudopotentials in a Generalized Eigenvalue Formalism. *Phys. Rev. B* **1990**, *41*, 7892.
(33) Kresse, G.; Hafner, J. Norm-Conserving and Ultrasoft Pseudopotentials for First-Row and Transition Elements. *J. Phys:. Condens. Matter* **1994**, *6*, 8245−8257.
(34) Monkhorst, H. J.; Pack, J. D. Special Points for Brillouin-Zone Integrations. *Phys. Rev. B* **1976**, *13*, 5188.
(35) Zhou, X.; Roehl, J. L.; Lind, C.; Khare, S. V. Study of B1 (NaCl-Type) to B2 (CsCl-Type) Pressure-Induced Structural Phase Transition in BaS, BaSe and BaTe Using Ab Initio Computations. *J. Phys.: Condens. Matter* **2013**, *25*, 075401.
(36) Zunic, T. B.; Vickovic, I. IVTON - A Program for the Calculation of Geometrical Aspects of Crystal Structures and Some Crystal Chemical Applications. *J. Appl. Crystallogr.* **1996**, *29*, 305.
(37) Lundegaard, L. F.; Miletich, R.; Balic-Zunic, T.; Makovicky, E. Equation of State and Crystal Structure of Sb_2S_3 between 0 and 10 GPa. *Phys. Chem. Miner.* **2003**, *30*, 463−468.
(38) Iwasaki, H.; Kikegawa, T. Structural Systematics of the High-Pressure Phases of Phosphorus, Arsenic, Antimony and Bismuth. *Acta Crystallogr. Sect. B* **1997**, *53*, 353−357.
(39) Olijnyk, H.; Nakano, S.; Takemura, K. First- and Second-Order Raman Scattering in Sb and Bi at High Pressure. *Phys. Status Solidi* **2007**, *244*, 3572−3582.
(40) Akahama, Y.; Kawamura, H.; Singh, A. K. Equation of State of Bismuth to 222 GPa and Comparison of Gold and Platinum Pressure Scales to 145 GPa. *J. Appl. Phys.* **2002**, *92*, 5892.
(41) Gerward, L.; Morup, S.; Topsoe, H. Particle Size and Strain Broadening in Energy-Dispersive X-ray Powder Patterns. *J. Appl. Phys.* **1976**, *47*, 822.
(42) Sharma, S. M.; Sikka, S. K. Pressure Induced Amorphization of Materials. *Progr. Mater. Sci.* **1996**, *40*, 1−77.
(43) Zhao, J.; Liu, H.; Ehm, L.; Chen, Z.; Sinogeikin, S.; Zhao, Y.; Gu, G. Pressure-Induced Disordered Substitution Alloy in Sb_2Te_3. *Inorg. Chem.* **2011**, *50*, 11291−11293.
(44) Ma, Y.; Liu, G.; Zhu, P.; Wang, H.; Wang, X.; Cui, Q.; Liu, J. Determinations of the High-Pressure Crystal Structures of Sb_2Te_3. *J. Phys.: Condens. Matter* **2012**, *24*, 475403.
(45) Stampfl, C.; Mannstadt, W.; Asahi, R.; Freeman, A. J. Electronic Structure and Physical Properties of Early Transition Metal Mononitrides: Density-Functional Theory LDA, GGA, and Screened-Exchange LDA FLAPW Calculations. *Phys. Rev. B* **2001**, *63*, 155106.
(46) Vilaplana, R.; Gomis, O.; Manjon, F. J.; Segura, A.; Perez-Gonzalez, E.; Rodriguez-Hernandez, P.; Munoz, A.; Gonzalez, J.; Marin-Borras, V.; Munoz-Sanjos, V.; et al. High-Pressure Vibrational and Optical Study of Bi_2Te_3. *Phys. Rev. B* **2011**, *84*, 104112.
(47) Vilaplana, R.; Santamaria-Perez, D.; Gomis, O.; Manjon, F. J.; Gonzalez, J.; Segura, A.; Munoz, A.; Rodriguez-Hernandez, P.; Perez-Gonzalez, E.; Marin-Borras, V.; et al. Structural and Vibrational Study of Bi_2Se_3 under High Pressure. *Phys. Rev. B* **2011**, *84*, 184110.

(48) Gomis, O.; Vilaplana, R.; Manjon, F. J.; Rodriguez-Hernandez, P.; Perez-Gonzalez, E.; Munoz, A.; Kucek, V.; Drasar, C. Lattice Dynamics of Sb_2Te_3 at High Pressures. *Phys. Rev. B* **2011**, *84*, 174305.
(49) Zhao, Y.; Chua, K. T. E.; Gan, C. K.; Zhang, J.; Peng, B.; Peng, Z.; Xiong, Q. Phonons in Bi_2S_3 Nanostructures: Raman Scattering and First-Principles Studies. *Phys. Rev. B* **2011**, *84*, 205330.
(50) Kharbish, S.; Libowitzky, E.; Beran, A. Raman Spectra of Isolated and Interconnected Pyramidal XS3 Groups (X = Sb,Bi) in Stibnite, Bismuthinite, Kermesite, Stephanite and Bournonite. *Eur. J. Miner.* **2009**, *21*, 325−333.
(51) Trentelman, K. A Note on the Characterization of Bismuth Black by Raman Microspectroscopy. *J. Raman Spectrosc.* **2009**, *40*, 585.
(52) Due to the existence of several broad and overlapping Raman bands in the spectra of $Bi2S_3$, a line width analysis will be highly unreliable.
(53) Chouinard, C.; Desgreniers, S. Bi_2O_3 under Hydrostatic Pressure: Observation of a Pressure-Induced Amorphization. *Solid State Commun.* **2000**, *113*, 125.
(54) Souza, S. M.; Poffo, C. M.; Triches, D. M.; de Lima, J. C.; Grandi, T. A.; Polian, A.; Gauthier, M. High Pressure Monoclinic Phases of Sb_2Te_3. *Physica B* **2012**, *407*, 3781.
(55) Degtyareva, O.; Hernandez, E. R.; Serrano, J.; Somayazulu, M.; Mao, H.-K.; Gregoryanz, E.; Hemley, R. J. Vibrational Dynamics and Stability of the High-Pressure Chain and Ring Phases in S and Se. *J. Chem. Phys.* **2007**, *126*, 84503.
(56) Schleid, T.; Lissner, F. A-Pr_2S_3, D-Ho_2S_3 and E-Yb_2S_3: Synthesis and Single Crystal Structure Investigations. *Z. Naturforsch., B: Chem. Sci.* **1996**, *51*, 733.
(57) Bera, A.; Pal, K.; Muthu, D. V. S.; Sen, S.; Guptasarma, P.; Waghmare, U. V; Sood, A. K. Sharp Raman Anomalies and Broken Adiabaticity at a Pressure Induced Transition from Band to Topological Insulator in Sb_2Se_3. *Phys. Rev. Lett.* **2013**, *110*, 107401.
(58) Larson, P. Effects of Uniaxial and Hydrostatic Pressure on the Valence Band Maximum in Sb_2Te_3: An Electronic Structure Study. *Phys. Rev. B* **2006**, *74*, 205113.
(59) Zhang, W.; Yu, R.; Zhang, H.-J.; Dai, X.; Fang, Z. First-Principles Studies of the Three-Dimensional Strong Topological Insulators Bi_2Te_3, Bi_2Se_3 and Sb_2Te_3. *New J. Phys.* **2010**, *12*, 65013.